Robotica (2013) volume 31, pp. 1221–1227. © Cambridge University Press 2013
doi:10.1017/S0263574713000398

# A passive dynamic walking model with Coulomb friction at the hip joint

Wenhao Guo†, Tianshu Wang†* and Qi Wang‡

†*School of Aerospace, Tsinghua University, Beijing 100084, China*
‡*Department of Dynamics and Control, Beihang University, Beijing 100191, China*

(Accepted April 11, 2013. First published online: May 23, 2013)

**SUMMARY**
This paper presents a modified passive dynamic walking model with hip friction. We add Coulomb friction to the hip joint of a two-dimensional straight-legged passive dynamic walker. The walking map is divided into two parts – the swing phase and the impact phase. Coulomb friction and impact make the model's dynamic equations nonlinear and non-smooth, and a numerical algorithm is given to deal with this model. We study the effects of hip friction on gait and obtain basins of attraction of different coefficients of friction.

KEYWORDS: Passive dynamic walking; Coulomb friction; Bipeds; Hip friction; Basin of attraction.

## 1. Introduction

The bipedal robot is one of the hottest points in the field of robotics for its better adapting to human living environments and more human-like walking gaits than other robots. The study of bipedal robot has achieved some results, such as QRIO[1] made by Sony and Asimo[2,3] presented by Honda. But these robots have lower energy efficiency compared with human walking and need higher requirements of controlling frequency and precision than required by human muscle.[4] Thus, new ideas are needed for the study of bipedal robots and understanding of human walking.

McGeer[5] first of all brought forward the concept of passive dynamic walking, which means bipedal walking without control and actuation. He represented a series of two-dimensional (2D) bipedal walkers that can walk down a gentle slope only powered by gravity. McGeer[5] proved that passive dynamic walking is feasible through numeral simulation and experiments. Garcia[7] demonstrated the simplest walking model and studied the relationship between the gait and the slope angle. Liu[9,11] made a systematic study of the gait of a straight leg planar passive walking model through simulations and experiments. Wisse[8] and Borzova and Hurmuzlu,[12] respectively, proved that the walking models with upper body could also walk stably. Qi *et al.*[13] presented a new planar passive dynamic model with contact between the feet and the ground. Based on insights of 2D prototypes, researchers[6,14] studied 3D passive dynamic walking machines.

Damping is unavoidable in engineering, but the influence of damping at the hip and knees of a passive dynamic walker has not been studied thoroughly. McGeer[5] introduced a walking model with linear damping at the hip joint and got a rough idea that even a small amount of friction in the hip joint can destroy the walking cycle. Goswami *et al.*[10] added a quadratic damper to a walking model by placing a motor implementing the same physical law. Goswami *et al.*'s[10] results reported that a walking model can possess extremely large limit-cycle attraction basins and can deal with steep slopes. Goswami *et al.*[10] and McGeer[5] got different results with different models. Compared with viscous and quadratic damping, Coulomb friction is closer to actual situations but harder to handle because the dynamical equations of the passive walker with Coulomb friction are non-smooth. We consider that it is significant to design a modified walking model with Coulomb friction at its hip and to study the friction's effects on the gait.

In this paper we present a planar, straight leg, passive dynamic walking model with Coulomb friction at the hip joint. After a detailed description of the model in Section 2, we give dynamical equations and numerical algorithm in Section 3. Next, simulation results and discussions are presented in Section 4. Finally, conclusions are made in Section 5.

## 2. The Model

We introduced Coulomb friction to the hip joint of a 2D straight-legged passive dynamic walking model (see Fig. 1). This passive walking model consists of two identical legs jointed by a hinge, which is not frictionless at the hip. The mass is concentrated at two points – on each leg, $m$, at a distance $c$ from the hip. The leg of length $l$ equals to 0.4 m whereas the length ratio, $r_c = \frac{c}{l}$. Each leg has a round foot of radius $R$ and the length ratio, $r_R = \frac{R}{l}$. This mechanism walks on a gentle ramp of slope $\gamma$.

Each step of this model is divided into two phases – the swing phase and the impact phase. During the swing phase, the stance leg rotates like an inverted pendulum.[5] The stance leg is in contact with the slope, while the other leg (the swing leg) is swinging around the hip joint (see Fig. 4). When the swing leg impacts the slope in front of the stance leg, it is the impact phase (see Fig. 3). We assume that the impact phase occurs instantaneously and the collision is inelastic. Our model is a modified version of the 2D straight-legged passive dynamic walking model presented by McGeer.[5]

* Corresponding author. E-mail: tswang@tsinghua.edu.cn

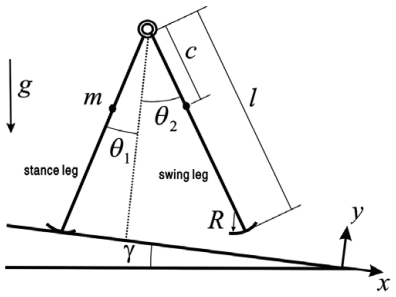


Fig. 1. The passive walking model.

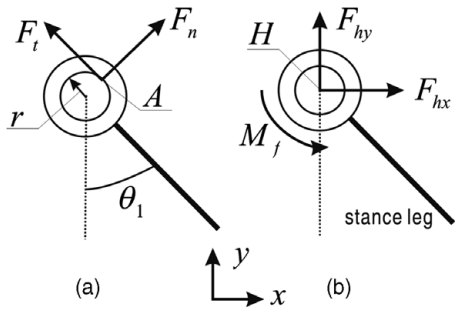


Fig. 2. The pivot force analysis.

## 3. The Walking Map

### *3.1. Coulomb friction of the hip joint*

The hip joint with Coulomb friction is the modification that makes our model different from the former ones. We consider the joint as a barrel hinge with Coulomb friction. The barrel connects to one leg and the pivot connects to the other. We mainly focus on the friction because of its prolonged effects on gait, so we think the clearance between the barrel and the pivot is negligible if the joint is processed precisely. Therefore, the hinge has only one degree of freedom (1 DOF). The force analysis of the pivot is shown in Fig. 2(a). The barrel and the pivot contact at point $A$. The normal force $F_n$ and the tangent force $F_t$ consist of the action of the barrel on the pivot. Radial load causes normal force ($F_n$). The tangent force, $F_t$, exists because of friction. According to the Coulomb friction model, $|F_t| \le \mu |F_n|$, where $\mu$ is the coefficient of friction.

Reduce $F_n$ and $F_t$ to the pivot center $H$ (see Fig. 2(b)), principal vector $\sum F$ and principal moment $M_f$ are obtained. The moment $M_f$ caused by friction should satisfy

$$M_f = r F_t, \tag{1}$$

where $r$ is the radius of the barrel. The principle vector $\sum F$ has two components – $F_{hx}$ parallel with the slope, and $F_{hy}$ vertical to the slope. Thus, the following equation should be satisfied:

$$\sum F = F_n + F_t = F_{hx} + F_{hy}. \tag{2}$$

The maximum frictional force $F_{\max}$ can be expressed as

$$F_{\max} = \mu |F_n|. \tag{3}$$

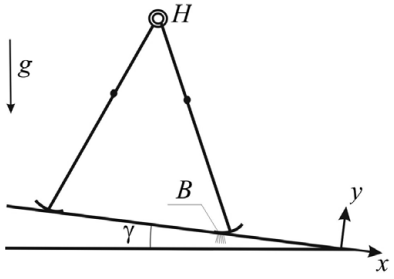


Fig. 3. The impact phase.

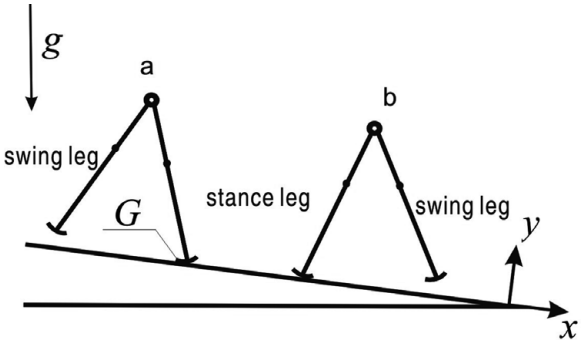


Fig. 4. The swing phase.

Correspondingly, we have the maximum frictional moment $M_{f\max} = r F_{\max}$. The moment of friction $M_f$ is always exerted in a direction that opposes movement or potential movement between the barrel and the pivot. It can be expressed as follows:

$$M_f = \begin{cases} M_{f\max}\operatorname{sgn}(\dot\theta_r) \dot\theta_r \ne 0 \text{(a)} \\ M_{f\max}\operatorname{sgn}(\ddot\theta_r) \dot\theta_r = 0 \text{ and } \ddot\theta_r \ne 0 \text{(b)} \\ \left(-M_{f\max}, M_{f\max}\right) \dot\theta_r = 0 \text{ and } \ddot\theta_r = 0 \text{(c)} \end{cases}. \tag{4}$$

The relative angular velocity, $\dot\theta_r = \dot\theta_2 - \dot\theta_1$, and the relative angular acceleration, $\ddot\theta_r = \ddot\theta_2 - \ddot\theta_1$. If the relative angular velocity $\dot\theta_r \ne 0$, the moment $M_f$ is caused by kinetic friction. If the relative angular velocity $\dot\theta_r = 0$, the moment of friction is static.

When Eqs. (4a) and (4b) are satisfied, we have $|F_t| = \mu |F_n|$. Note that $F_n \perp F_t$ and $F_{hx} \perp F_{hy}$ and using Eqs. (2) and (3) it is not hard to obtain the following equation:

$$F_{\max} = \frac{\mu}{\sqrt{1+\mu^2}} \sqrt{F_{hx}^2 + F_{hy}^2}. \tag{5}$$

### *3.2. Dynamic equations of the impact phase*

When $\theta_1 + \theta_2 = 0$, foot strike occurs. Angular momentum of the whole machine about the point of collision $L_f$ is conservative, which is the same as that of McGeer's model.[5] $L_f$ is a function of $\theta_1$, $\theta_2$, $\dot\theta_1$, $\dot\theta_2$. This can be mathematically expressed as

$$L_f^-(\theta_1,\ \theta_2,\ \dot\theta_1^-,\ \dot\theta_2^-) = L_f^+(\theta_1,\ \theta_2,\ \dot\theta_1^+,\ \dot\theta_2^+). \tag{6}$$

Pre- and post-impacts are denoted by "−" and "+" respectively. But angular momentum of the tailing leg about

https://doi.org/10.1017/S0263574713000398 Published online by Cambridge University Press

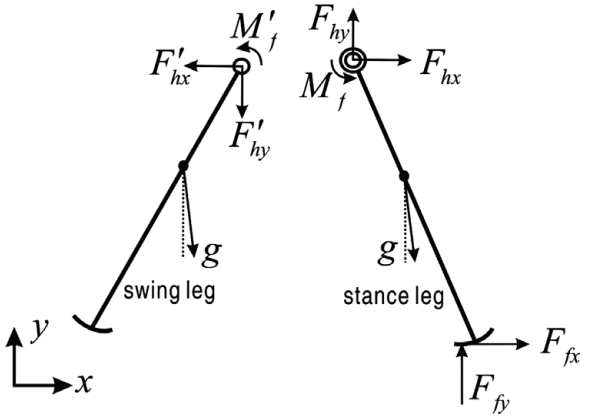


Fig. 5. Swing force analysis.

the hip is not conservative anymore. The reason is that the friction moment $M_f$ is directly proportional to the principle vector $\sum F_n$, which is a considerably huge magnitude force when heel strike happens. So $M_f$ is non-ignorable, and the angular momentums of the tailing leg about the hip $L_h$ pre- and post-impacts are not the same.

Study the momentum of the tailing leg during the impact phase, the only force non-ignorable acting on the tailing leg is $\sum F$. According to the theorem of momentum,

$$\begin{cases} P_x^+ - P_x^- = I_x \\ P_y^+ - P_y^- = I_y \end{cases}, \tag{7}$$

where $P_x$ and $P_y$ are the projections of the tailing leg's momentum on $x$ and $y$axes respectively. $I_x$ and $I_y$ consist of the impulse of the principle vector $\sum F$. Assuming that impact happens in a very short time $\Delta t$, which is infinitesimal, then $I_x$ and $I_y$ can be expressed as

$$\begin{cases} I_x = F_{hx}\Delta t \\ I_y = F_{hy}\Delta t \end{cases}. \tag{8}$$

Angular momentum of the tailing leg about the hip $L_h$ satisfies

$$L_h^+(\theta_1,\ \theta_2,\ \dot\theta_1^+,\ \dot\theta_2^+) - L_h^-(\theta_1,\ \theta_2,\ \dot\theta_1^-,\ \dot\theta_2^-) = -M_f\Delta t. \tag{9}$$

Substituting Eqs. (5) and (8) into Eq. (9),

$$L_h^+(\theta_1,\theta_2,\dot\theta_1^+,\dot\theta_2^+) - L_h^-(\theta_1,\theta_2,\dot\theta_1^-,\dot\theta_2^-) = -\frac{\mu r}{\sqrt{1+\mu^2}}\mathrm{sgn}(\dot\theta_r^+ - \dot\theta_r^-). \tag{10}$$

Equations (6), (7) and (10) are all nonlinear equations about $\dot\theta_1^+$, $\dot\theta_2^+$, $I_x$ and $I_y$. The Newton–Raphson method can be used to deal with these nonlinear algebraic equations numerically.

### *3.3. Dynamic equations of the swing phase*

The force analysis of each leg during the swing phase is shown in Fig. 5.

Table I. Unknown parameters.

| Number | 1 | 2 | 3 | 4 | 5 | 6 | 7 | 8 | 9 | 10 |
|---|---|---|---|---|---|---|---|---|---|---|
| Parameters | $\ddot x_{c1}$ | $\ddot y_{c1}$ | $\ddot x_{c2}$ | $\ddot y_{c2}$ | $\ddot\theta_1$ | $\ddot\theta_2$ | $F_{hx}$ | $F_{hy}$ | $F_{fx}$ | $F_{fy}$ |

The dynamic equations are

$$\begin{cases} m\ddot x_{c1} = \mathrm{mg}\sin\gamma + F_{fx} + F_{hx} \\ m\ddot y_{c1} = -\mathrm{mg}\cos\gamma + F_{fy} + F_{hy} \\ J_c\ddot\theta_1 = M_f + F_{fx}[R + (l-c-R)\cos\theta_1] \\ \quad + F_{y1}(l-c-R)\sin\theta_1 - F_{hx}c\cos\theta_1 - F_{hy}c\sin\theta_1, \\ m\ddot x_{c2} = \mathrm{mg}\sin\gamma - F_{hx} \\ m\ddot y_{c2} = -\mathrm{mg}\cos\gamma - F_{hy} \\ J_c\ddot\theta_2 = -M_f + F_{hx}c\cos\theta_2 + F_{hy}c\sin\theta_2 \end{cases} \tag{11}$$

where $J_c$ is the moment of inertia of each leg with respect to its mass center. $x_{ci}$ and $y_{ci}(i = 1, 2)$ denote the position of mass center of leg $i$. The constraint force offered by the slope to the stance leg consists of $F_{fx}$ and $F_{fy}$. The mathematical expression of $M_f$ is Eq. (4). In the swing phase, the stance foot rolls on the slope without slip, thus the following constraint equations are satisfied:

$$\begin{cases} x_{c1} = -(l-c-R)\sin\theta_1 - R\theta_1 + x_0 \\ y_{c1} = (l-c-R)\cos\theta_1 + R + y_0 \\ x_{c2} = -(l-R)\sin\theta_1 - R\theta_1 + c\sin\theta_2 + x_0 \\ y_{c2} = (l-R)\cos\theta_1 + R - c\cos\theta_2 + y_0 \end{cases}. \tag{12}$$

Let the stance foot and the slope contact at point $G$. $(x_0,\ y_0)$ is the position of $G$ when the stance leg is vertical to the slope $(\theta_1 = 0)$.

It is necessary to make a detailed description of the algorithm method that we used for simulation because the dynamic equations of the swing phase are nonlinear and non-smooth. We mainly use Eqs. (4) and (11) and the second derivative of Eq. (12) to simulate this walker's swing phase. The unknown parameters are listed in Table I. The following three conditions have to be considered: (a) When Eq. (4a) is satisfied, $M_f$ is a function of $F_{hx}$, $F_{hy}$, $\dot\theta_1$ and $\dot\theta_2$. The Newton–Raphson method can be used to deal with the nonlinear algebraic equations. (b) When Eq. (4b) is satisfied, $M_f$ is a function of $F_{hx}$, $F_{hy}$, $\ddot\theta_1$ and $\ddot\theta_2$. But $\ddot\theta_1$ and $\ddot\theta_2$ are unknown parameters. Note that sign function $\mathrm{sgn}(\ddot\theta_r) = \mathrm{sgn}(\ddot\theta_2 - \ddot\theta_1)$ is the only function using $\ddot\theta_1$ and $\ddot\theta_2$, we use try-and-error method. First, assume $\mathrm{sgn}(\ddot\theta_2 - \ddot\theta_1) = 1$ (or $\mathrm{sgn}(\ddot\theta_2 - \ddot\theta_1) = -1$), then use Newton–Raphson's method to obtain the value of $\ddot\theta_1$ and $\ddot\theta_2$. Check whether numerical results agree with the assumptions. If the answer is negative, change another assumption; if the answer is positive, stop trying. (c) When Eq. (4c) is satisfied, it means the walker has only 1 DOF, and new dynamic equations which are easier than the equations of conditions (a) and (b) are needed.

https://doi.org/10.1017/S0263574713000398 Published online by Cambridge University Press

Table II. Value of parameters.

| Model parameters | $l(m)$ | $r_c$ | $r_R$ | m (kg) | $J_c$(kg m$^2$) | $g$ (m/s$^2$) | $r$ (m) |
|---|---|---|---|---|---|---|---|
| Value | 0.4 | 0.25 | 0.25 | 1 | 0.008 | 9.8 | 0.005 |

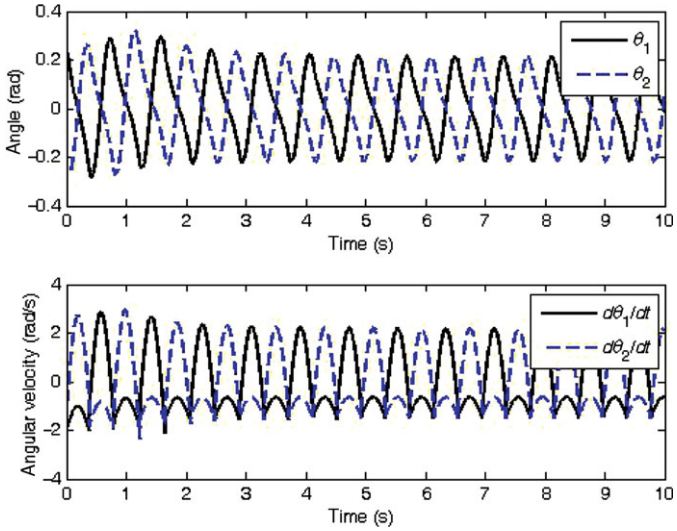


Fig. 6. (Colour online) The time history of $\theta_i$ and $\dot{\theta}_i$ $(i = 1, 2)$.

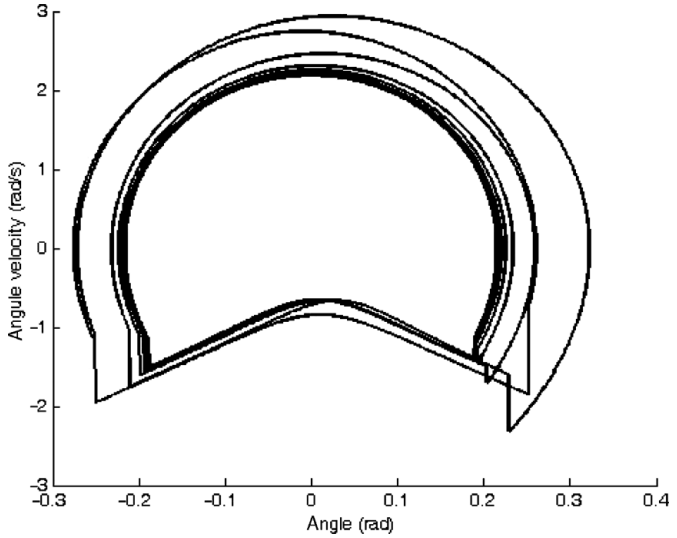


Fig. 7. The phase diagram of leg 1.

## 4. Results and Discussions

### *4.1. Existence of stable gait*

The values of model parameters used for simulation are listed in Table II. The other parameters, such as angle of the slope, initial conditions and the coefficient of friction, will be listed in later simulation examples.

Let the angle of the slope $\gamma = 0.01$ rad, the coefficient of friction $\mu = 0.05$ and the initial condition $[\theta_1,\ \theta_2,\ \dot{\theta}_1,\ \dot{\theta}_2] = [0.254,\ -0.2541,\ -1.954,\ -1.118]$, then a stable gait is obtained. The time history of two legs is shown in Fig. 6. Figure 7 is the phase diagram of one leg. A few steps after start, the leg's phase trajectory converges to a stable limit circle. That means the walker does have a one-period

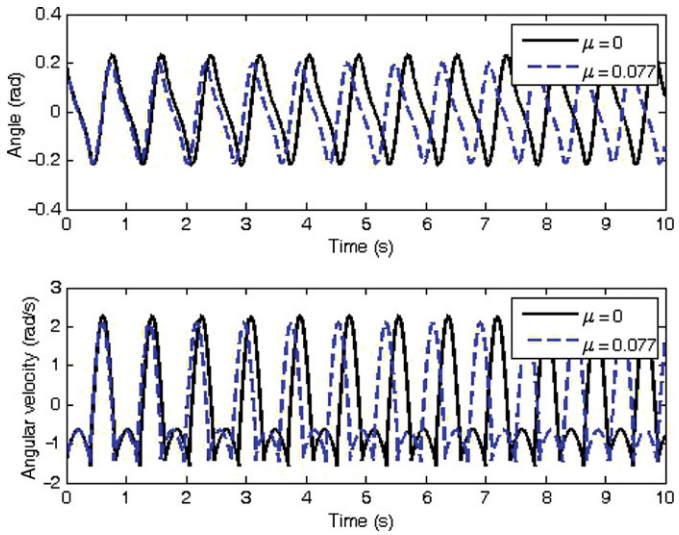


Fig. 8. (Colour online) The time history of angles and angular velocities with different friction coefficients.

stable gait even introducing Coulomb friction ($\mu = 0.05$) to its hip.

The gait in Fig. 6 is one of the typical stable gaits that we found via numerical simulation, and it is necessary to explain how these gaits are obtained. For a given $\gamma$, the existence of stable gaits has been studied by former researchers[5,9,10] with $\mu = 0$ (frictionless hip joint). We increase $\mu$ from 0 to a very small positive number $\Delta\mu$ and set the initial condition as the stable gait of $\mu = 0$, the stable gait of the walker with small hip friction ($\mu = \Delta\mu$) is obtained after a few steps. Then we rise $\mu$ to a larger number and set the initial condition as the stable gait of $\mu = \Delta\mu$, another stable gait will be found soon. This cyclic process until the stable gait disappears. Then we can find a range of $\mu$ to study the effects of friction on the stable gait. Two different coefficients of friction, $\mu = 0$ and 0.077, are chosen for comparison. The time history of angles of different coefficients of friction is shown in Fig. 8. The comparison of limit cycles of these two stable gaits is shown in Fig. 9. The maximum step amplitude and period decrease with increasing coefficient of friction (see Fig. 10). Goswami *et al.*[10] also got similar results.

With rise of $\mu$ from 0.077 to 0.085, the walker has no stable gait on the slope of angle $\gamma = 0.01$ rad (Fig. 11). The reason is that friction and impact cost more energy than the amount of gravitational potential energy that the walker loses per step. With increase of $\gamma$ from 0.01 to 0.015 rad, we again find a stable gait. The simulation results of the newly found stable gait are shown in Figs. 12 and 13. When $\mu = 0.085$, Fig. 14 shows the average speed of the stable gait versus $\gamma$. Stable gaits exit when $\gamma \geq 0.013$ rad. Friction makes the walker unable to walk on slopes of smaller angles.

### *4.2. Basin of attraction*

The existence of a stable gait does not guarantee that every time a passive walker can walk on a slope, the initial condition should also be considered. If a walker starts walking with a bad initial condition, its gait will not converge to the stable gait and will finally fall. On the other hand, if a proper initial condition is given, the walker will walk permanently

https://doi.org/10.1017/S0263574713000398 Published online by Cambridge University Press

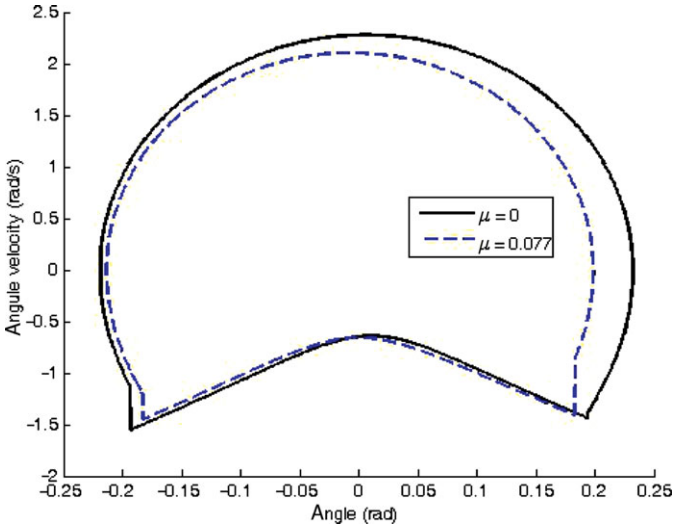


Fig. 9. (Colour online) The limit cycles of different gaits with different friction coefficients.

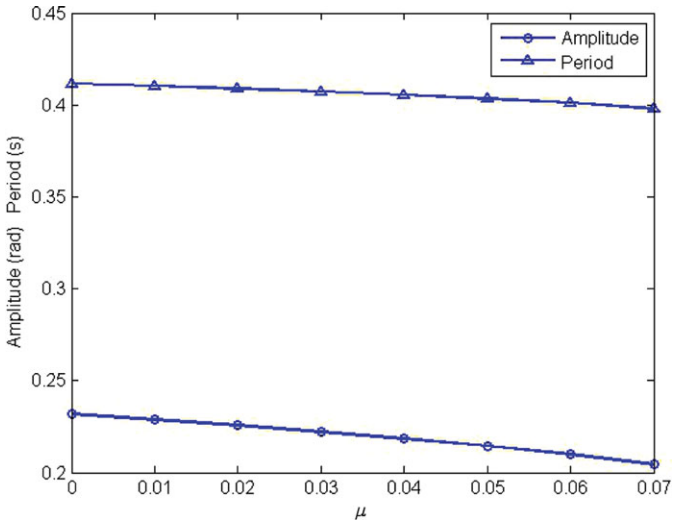


Fig. 10. (Colour online) The plots of amplitude and period as a function of $\mu$.

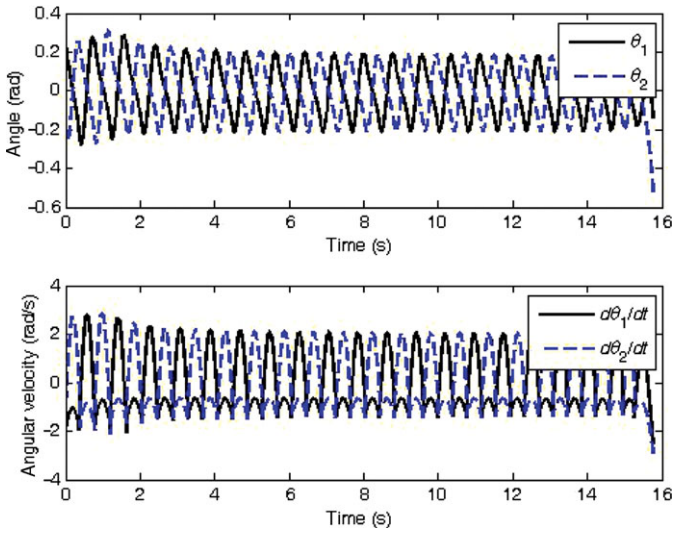


Fig. 11. (Colour online) The time history of $\theta_i$ and $\dot{\theta}_i$ $(i = 1, 2)$.

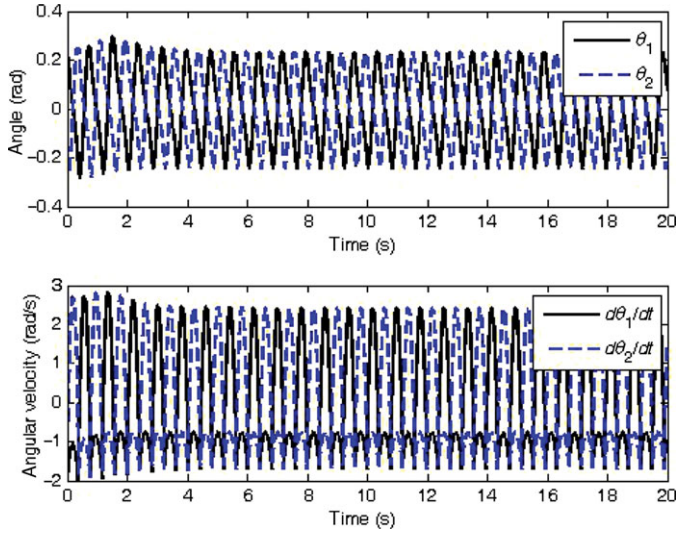


Fig. 12. (Colour online) The time history of $\theta_i$ and $\dot{\theta}_i$ $(i = 1, 2)$.

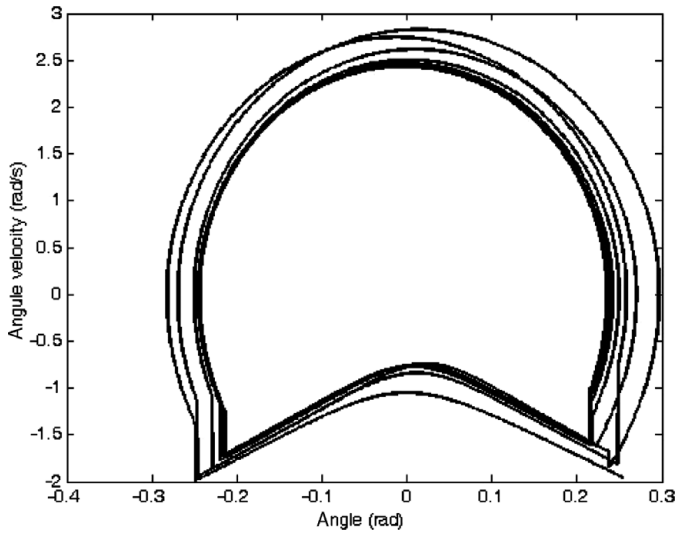


Fig. 13. The phase diagram of leg 1 with $\mu = 0.085$.

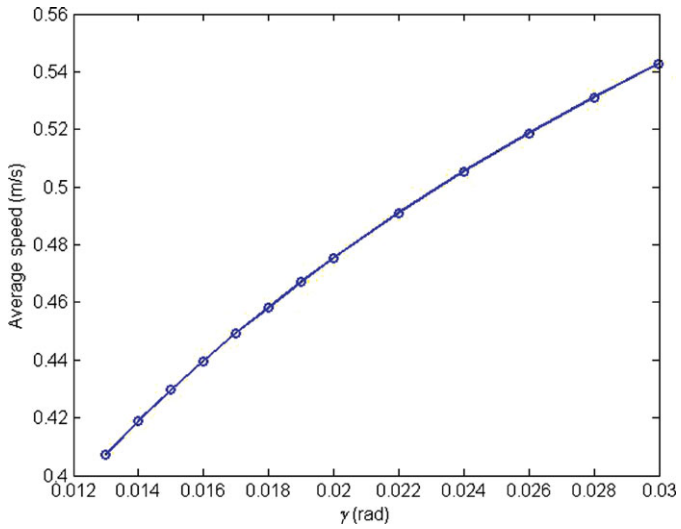


Fig. 14. (Colour online) The average velocity of stable gait versus $\gamma$.

https://doi.org/10.1017/S0263574713000398 Published online by Cambridge University Press

on the condition that the slope is long enough. All proper initial conditions in the phase space consist of the basin of attraction of a passive walker. The size of a walker's basin of attraction reflects its sensitivity to initial conditions. The basin of attraction of a walking model with Coulomb friction at the hip is also studied in this paper.

We use cell mapping method to determine the basin of attraction of our new walking model. The cell mapping method was originally presented by Hsu.[15] Using the cell mapping method, portion of phase space, which may include feasible initial conditions of a nonlinear system, is discrete into a finite number of cells. Then the dynamics of the system can be expressed in the form of a mapping sequence from one cell to another. This method indeed reduces some computation but cuts down the accuracy within the acceptable range. Schwab and Wisse[16] have used the cell mapping method to study the simplest passive model and find that the basin of attraction is a small, thin area.

Considering that all feasible gaits have the same special state $\theta_1 = -\theta_2$, we chose the Pioncaré section at the moment right after heel strike. Then the dimension of the phase space that we focus on reduces from four $(\theta_1, \theta_2, \dot{\theta}_1, \dot{\theta}_2)$ to three $(\theta_1, \dot{\theta}_1, \dot{\theta}_2)$ and we can spend much less time on computation. Another thing we have pointed out is that not all the phase space is significant for us, for example it is impossible that the angle of the stance leg is greater than $\frac{\pi}{2}$. So the basin's position and size have to be considered when choosing which part of the phase space should be studied. Calculating work is another thing that affects our decision of the range of significant phase space. The size of a cell must be small enough, or the results' accuracy will be unacceptable. Thus, the larger the phase space to be studied, the more the calculating work to be done. The range we chose to study is $\theta_1 \in (0, 1)$ (rad), $\dot{\theta}_1 \in (-3, 1)$ (rad/s), $\dot{\theta}_2 \in (-3, 1)$ (rad/s), and the size of the cell is 0.01 (rad) $\times$ 0.04 (rad/s) $\times$ 0.04 (rad/s).

The basin of attraction with $\mu = 0$ and its projections are shown in Fig. 15. Choose any point in the basin as the initial condition, the walker can converge to the fixed point (0.1936, −1.4355, −1.1179). Set the initial condition as (0.54, −3, −2.72), then the walker represents a stable gait after 21 steps of adjustment (see Table III). In order to

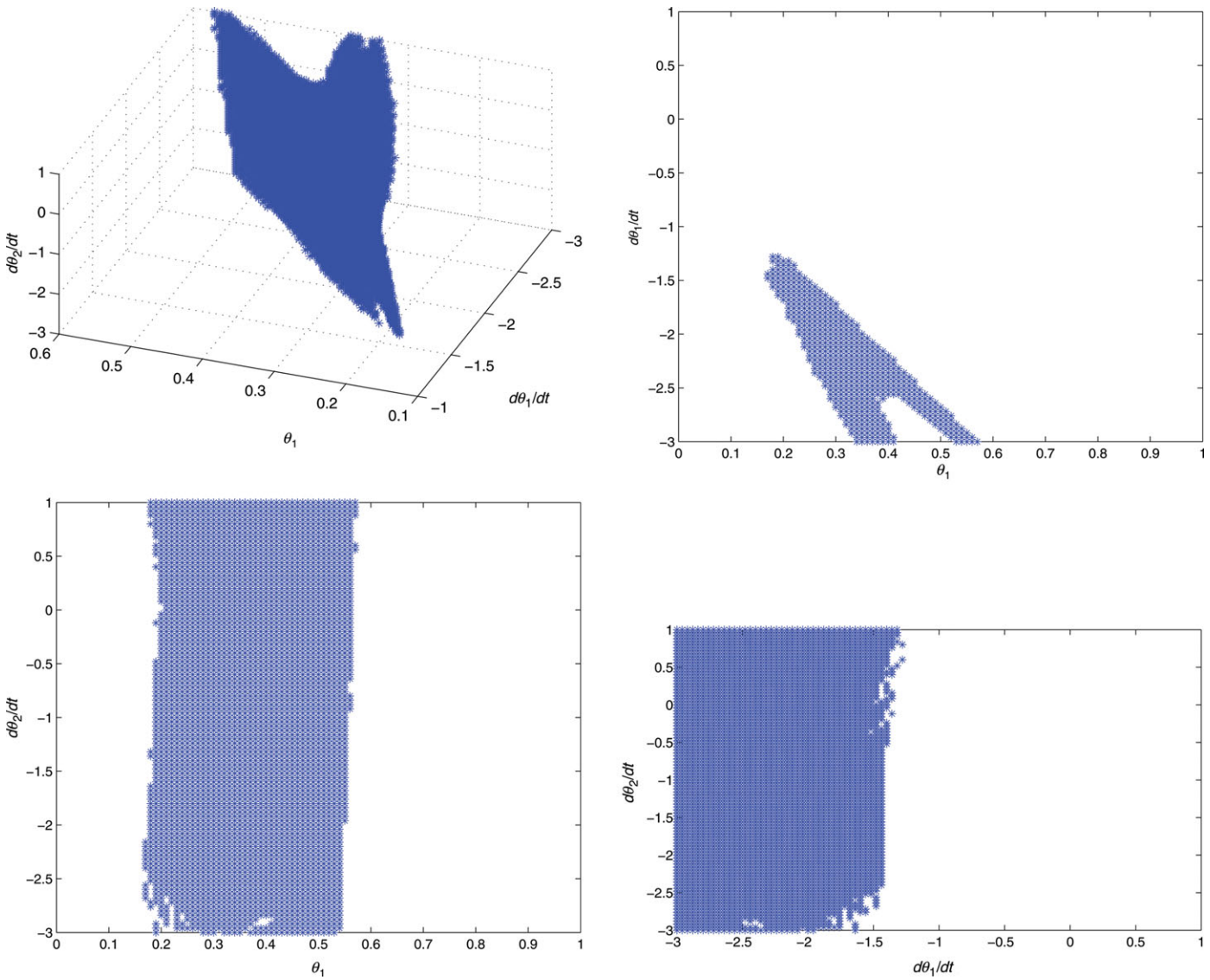


Fig. 15. (Colour online) The basin of attraction with $\mu = 0$.

https://doi.org/10.1017/S0263574713000398 Published online by Cambridge University Press

Table III. Adjusting steps.

| Step | $\theta_1$ (rad) | $\dot{\theta}_1$ (rad/s) | $\dot{\theta}_2$ (rad/s) |
|---|---|---|---|
| 0 | 0.54 | −3 | −2.72 |
| 1 | 0.2256 | −1.5453 | −0.2296 |
| 2 | 0.2119 | −1.5655 | −1.0302 |
| 3 | 0.2115 | −1.5507 | −1.1490 |
| ... | ... | ... | ... |
| 4 | 0.1936 | −1.4356 | −1.1178 |
| 5 | 0.1936 | −1.4355 | −1.1179 |
| 6 | 0.1936 | −1.4355 | −1.1179 |

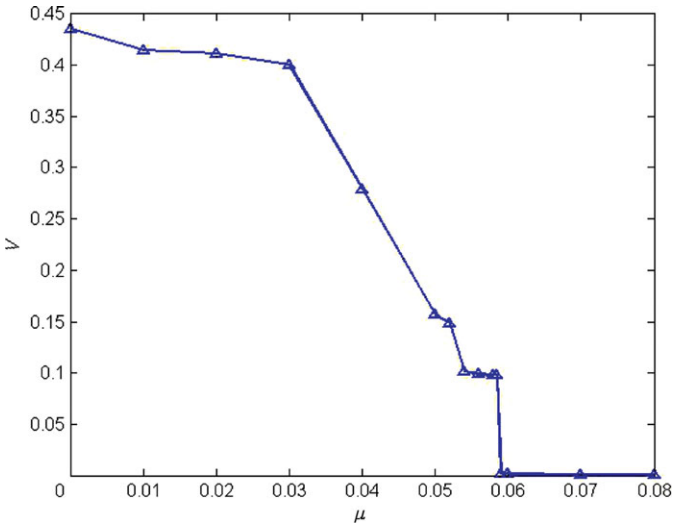


Fig. 16. (Colour online) The volume of basin $V$ versus $\mu$.

study the effects of friction on the basin of attraction, we use a generalized volume $V = \theta \times \dot{\theta}_1 \times \dot{\theta}_2$ to stand for the size of the basin. The generalized volume, $V$ decreases with the rise of $\mu$ (see Fig. 16). The hip friction plays a negative role to the walker's robustness. It is contrary to Goswami *et al.*'s results.[10] On the other hand, the stable gait is not as sensitive as claimed by McGeer.[5]

## 5. Conclusions and the Future Work

In this paper we introduced Coulomb friction to the hip joint of a 2D straight-legged passive walker. The main aim of the research was to analyze the effects of the hip friction on the gait. The Newton–Raphson method and the try-and-error method were used to deal with the nonlinear and non-smooth dynamical equations. With the aid of the cell mapping method, we obtained basins of attraction for different $\mu$.

We can conclude as follows:

- A passive walker with Coulomb friction at hip does have stable gaits when $\mu$ belongs to an appropriate range.
- The maximum step amplitude and period decrease when the friction coefficient increases.
- Because of hip friction the walker is unable to walk on slopes of smaller angles.
- The basin of attraction becomes smaller when $\mu$ becomes bigger. Hip friction makes the walker more sensitive to initial conditions.

In the future work, knees with friction can be added to the present model and the effects of knee friction will be studied.

## Acknowledgments

This research is funded by the National Natural Science Foundation of China (10872102, 11072014).

## References

1. T. Ishida, "Development of a Small Biped Entertainment Robot QRIO," **In**: *Proceedings of the 2004 International Symposium on Micro-NanoMechatronics and Human Science*, Nagoya, Japan (IEEE, New York, 2004) pp. 23–28.
2. Y. Sakagami, R. Watanabe and C. Aoyama, "The Intelligent ASIMO: System Overview and Integration," **In**: *Proceedings of the IEEE International Conference on Intelligent Robots and Systems*, Piscataway, New Jersey (IEEE, New York, 2002) pp. 2478–2483.
3. K. Hirai, M. Hirose, Y. Haikawa, "Development of Honda Humanoid Robot," **In**: *Proceedings of the IEEE International Conference on Robotics and Automation*, New Jersey (IEEE, New York, 1998) pp. 1321–1326.
4. F. E. Zajac, "Muscle and tendon: Properties, models, scaling, and application to biomechanics and motor control," *Crit. Rev. Biomed. Eng.* 17(4), 359–411 (1989).
5. T. McGeer, "Passive dynamic walking," *Int. J. Robot. Res.* **9**(2), 62–82 (Apr. 1990).
6. S. Collins, M. Wisse and A Ruina, "A three-dimensional passive-dynamic walking robot with two legs and knees," *Int. J. Robot. Res.* **20**(7), 607–615 (2001).
7. M. Garcia, "Passive Dynamic Models of Human Gait," *Poster Abstract from Engineering Foundation Conference on Biomechanics and Neural Control of Human Movement*, Mt. Sterling, Ohio (1996).
8. M. Wisse, "Three Additions to Passive Dynamic Walking: Actuation, an Upper Body, and 3D Stability," **In**: *Proceedings of the IEEE International Conference on Humanoid Robots*, New Jersey (IEEE, New York, 2004) pp. 113–132.
9. N. Liu, *Simulation and Experimental Study on the Dynamics of Passive Bipedal Walker* (Tsinghua University, Beijing, China, 2009).
10. A. Goswami, B. Thuilot and B. Espiau, "A study of the passive gait of a compass-like biped robot: Symmetry and chaos," *Int. J. Robot. Res.* **17**(12), 1282–1301 (1998).
11. N. Liu, J. Li and T. Wang, "Study of the basin of attraction of passive models by the aid of cell-to-cell mapping method," *Engeering Mech.* **25**(10), 218–223 (2008).
12. E. Borzova and Y. Hurmuzlu, "Passively walking five-link robot," *Automatica* **40**(4), 621–629 (2004).
13. F. Qi, T. Wang and J. Li, "The elastic contact influences on passive walking gaits," *Robotica* **29**(5), 787–796 (2011).
14. Q. Wang, Y. Huang and L. Wang, "Passive dynamic walking with flat feet and ankle compliance," *Robotica* **28**(3), 413–425 (2010).
15. C. S. Hsu, "A theory of cell-to-cell mapping dynamical systems," *J. Appl. Mech.* **47**, 913–939 (1980).
16. M. Wisse, A. L. Schwab, F. C. T. van der Helm, "Passive Dynamic Walking Model with Upper Body," *Robotica* **22**(6), 681–688 (2004).

https://doi.org/10.1017/S0263574713000398 Published online by Cambridge University Press